ISSN 1063-7710, Acoustical Physics, 2019, Vol. 65, No. 6, pp. 652–657. © Pleiades Publishing, Ltd., 2019.

PHYSICAL ACOUSTICS

Surface Acoustic Wave Characteristics with a Layered Structure of IDT/θ° YX-$LiTaO_3$/SiO_2/AlN/diamond

Q. Xiao[a], M. Dai[b], J. Chen[a], Y. P. Fan[c], P. Cai[a], and X. J. Ji[a,*]

[a] *School of Electronic Information and Electrical Engineering, Shanghai Jiao Tong University, Shanghai, 200240 P.R. China*

[b] *No. 704 Research Institute, China Shipbuilding Industry Corporation, Shanghai, 200031 P.R. China*

[c] *School of Optical-Electrical and Computer Engineering, University of Shanghai for Science and Technology, Shanghai, 200093 P.R. China*

**e-mail: jxj127@sjtu.edu.cn*

Received November 3, 2018; revised March 21, 2019; accepted July 9, 2019

Abstract—A new layered surface acoustic wave (SAW) structure was proposed by Murata Co., Ltd recently. It was reported that such structure could achieve an incredible high performance including a higher quality factor Q and electromechanical coupling coefficient K^2. For deeply understanding propagating characteristics and optimizing the performance of the SAWs in such structure, a layered structure of IDT/θ° YX-$LiTaO_3$/SiO_2/AlN/Diamond with different structural parameters were theoretically investigated by FEM method. The calculated admittance shows that four eigenmodes simultaneously exist in such layered structure including the main mode SH SAW. And compared with the Traditional SAW structure, the main mode could achieve a higher value of K^2 with sacrificing its velocity a little. Different metal layers (Au, Al, and Cu) were examined as the electrode material. With Au employed, the K^2 of the main mode is a little larger resulting from better suppression of the spurious modes. The optimum thickness of electrode and piezoelectric layer are 0.2 and 0.02λ, respectively. In this case, the K^2 for the SH SAW achieves its maximum value of 12.20% with a large phase velocity of 3608 m/s. Furthermore, the pure SH SAW can be obtained with the Y-cut Euler angle θ from 0° to 60°, where its K^2 has a wide range of 8.70 to 13.69%. Consequently, the work provides a theoretical guide for designing SAW devices of different bandwidth and operation frequency with such structure.

Keywords: surface acoustic wave, layered structure, high performance, structure optimization

DOI: 10.1134/S1063771019060150

INTRODUCTION

Surface acoustic wave (SAW) devices have expanded into diverse application fields such as filters, sensors and radio frequency identification (RFID) tags because of their excellent characteristics, including low insertion, small size and reasonable cost [1, 2]. For near future, the demands for SAW devices are the further improvement of the quality factor (Q), electromechanical coupling coefficient (K^2), device linearity, temperature stability and so on [3]. Numerous studies have been conducted on improving these performances. To improve the temperature stability, temperature compensated SAW (TC-SAW) has been developed [4–8]. To improve the phase velocity and K^2, wafer bonding technique and new materials have been introduced [9–11]. To achieve high Q value, piston mode and length-weighted dummy electrodes techniques have been developed [12–14]. Recently, an Incredible High Performance (IHP) SAW structure was proposed by Murata Co. [15]. Such new structure could achieve incredible high performance of SAW devices and thus draw much attentions. However, the Ref. [15] focused on energy confinement and temperature compensation by optimizing the thickness of the acoustic reflector stack. The more detailed SAWs propagating characteristics on such structure, changing with the other structural parameters (i.e. electrode thickness, cuts of piezoelectric layer), haven't been reported.

Therefore, the authors deeply investigated the dependences of K^2 and phase velocities of the different modes propagating in the IHP SAW structure of IDT/θ° YX-LT/SiO_2/AlN/Diamond with different electrode materials and structural parameters, where diamond was employed as the support substrate to achieve enlarged phase velocity [16]. Firstly, the relative input admittance of the SAWs propagating on the IHP SAW structure and Traditional SAW (IDT/θ° YX-LT/Diamond) structure were calculated, respectively. Then, the authors calculated displacement filed distribution for each mode, and evaluated the K^2, phase velocities with different interdigital transducer (IDT) materials. Finally, such characteristics was also

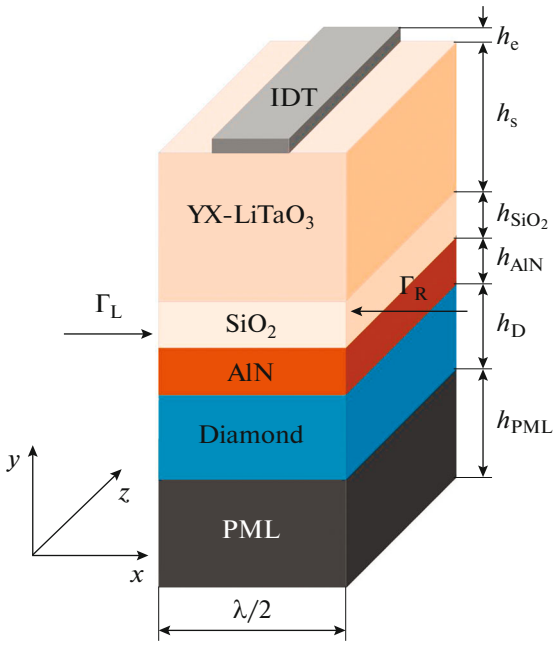

Fig. 1. Quasi-3D periodic FEM model used in the simulation (not to scale).

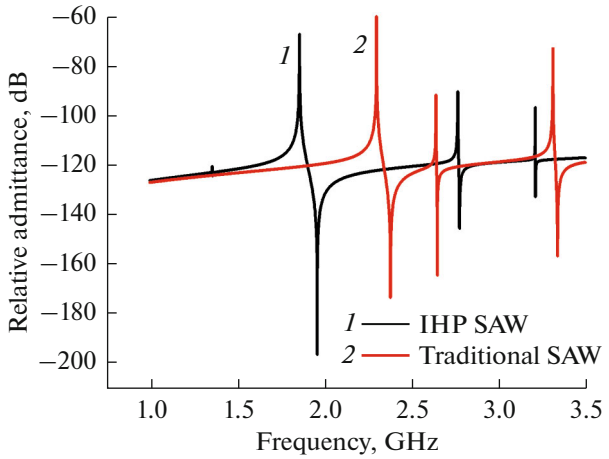

Fig. 2. Relative admittance of infinitely long IDTs on the Traditional and IHP SAW structures.

evaluated with different layer thickness and Y-cut Euler angle.

It is noteworthy to mention that the authors have previously investigated the characteristics of the two types of SAWs with different structural parameters in the similar structure [17]. In this paper, the authors investigate characteristics of all the four eigenmodes in such structure and optimize the performance by suppression of the spurious modes.

MODELING AND SIMULATION

In this paper, calculations were conducted by the Finite Element Method (FEM) with the commercial software package COMSOL Multiphysics. Figure 1 shows quasi-3D periodic FEM model used in the simulation.

Six layers existed in this model. The layers of SiO_2 and AlN were employed to build a Bragg reflector stack. The diamond was employed as support substrate to achieve enlarged phase velocity. And the perfectly matched layer (PML) was placed at the bottom of the support substrate to avoid wave reflection from the bottom. The thickness of each layer were respectively denoted as h_e, h_s, h_{SiO_2}, h_{AlN}, h_D and h_{PML}.

The authors also give a brief description of the manufacturing procedure of such a layered structure. Firstly, the SiO_2 and AlN film were deposited by the RF reactive magnetron sputtering process on the support substrate diamond [18, 19]. Then, the handle wafer (SiO_2/AlN/Diamond) and the donor wafer (YX-LT) were cleaned and bonded together based on ion implantation and wafer bonding [20]. Finally, a chemical-mechanical-polishing (CMP) process is adopted to smooth the surface of the YX-LT thin film, and IDTs were deposited on the smoothed surface using photolithographic process [21].

In this model, the wavelength λ was 2 μm. The h_D and h_{PML} were 2λ and λ, respectively. The h_{SiO_2} and h_{AlN} were both 0.25λ. Only a half period was considered and the field variables at the left (Γ_L) and right (Γ_R) surfaces were set as antisymmetric periodic. Harmonic analysis was conducted with 1 V loaded to the IDT.

Figure 2 presents the calculated relative admittance of infinitely long IDTs on the Traditional and IHP SAW structures as a function of frequency, respectively, where the IDT material is Au, $h_e = 0.015\ \lambda$, $h_s = 0.2\ \lambda$, $\theta = 42°$. It is clear that four eigenmodes simultaneously exist in such kind of IHP SAW structure. The admittance amplitude of each mode indicates that the second mode is the main mode. Additionally, it also indicates that the main mode in the IHP SAW structure can be more efficiently excited with better suppression of the spurious modes. Then, the K^2 of each mode in the two different structures was estimated by the following formula derived from the equivalent circuit analysis [22]:

$$K^2 = \frac{\pi f_r/2f_a}{\tan(\pi f_r/2f_a)}. \quad (1)$$

The calculated results show that the K^2 of the main mode in the IHP SAW structure was 12.19%, much higher than 8.02%, the K^2 of the main mode in the Traditional SAW structure. On the other hand, the velocities of the main mode in the IHP SAW structure decreased a little, derived by $V_r = f_r\lambda$, $V_a = f_a\lambda$. The frequencies of f_r and f_a for each eigenmode were obtained for $Y(f)^{-1} = 0$ and $Y(f) = 0$, respectively.

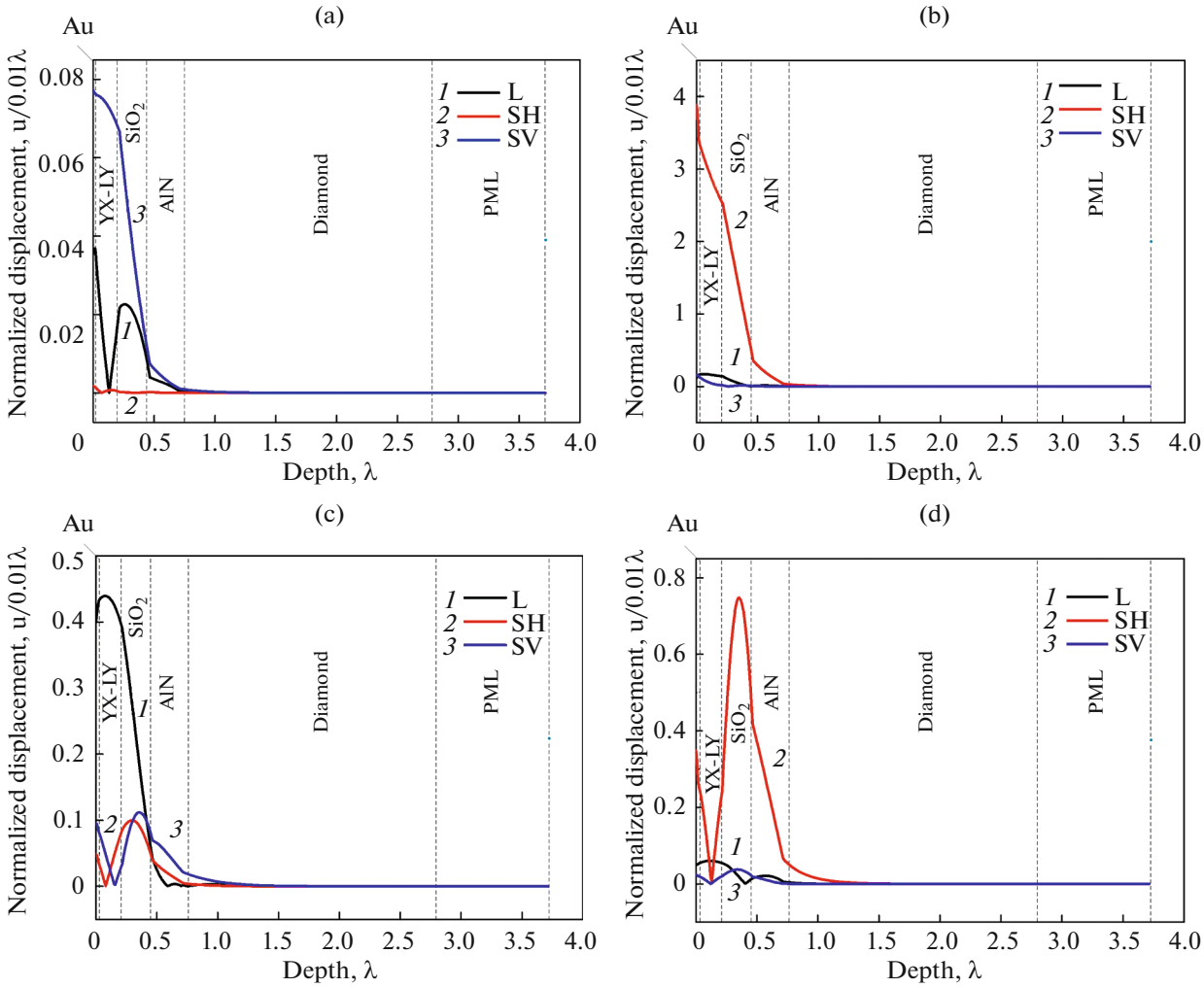

Fig. 3. Normalized displacement field distributions along the depth of the layered structure for the different eigenmodes: (a)—the 1st mode, (b)—the 2nd mode, (c)—the 3rd mode, (d)—the 4th mode.

Furthermore, the normalized displacement field distributions along the depth were calculated to identity each eigenmode, as depicted in Figs. 3a–3d.

The displacement field of the first mode are mainly composed of longitudinal (L) and shear vertical (SV) components; the second and fourth modes are mainly composed of shear horizontal (SH) component; the third mode is mainly composed of L component. Thus, the first mode is the typical Rayleigh SAW; the second mode is SH SAW; the third and fourth modes can be categorized as longitudinal wave and high-order SH wave, respectively.

Besides, from the amplitude of the displacements, we could conclude that the first three modes concentrated most of their energies in the IDTs and YX-LT layers, whereas the fourth mode concentrated that in the SiO_2 layer because of the reflection from boundaries [23, 24]. This indicates that the acoustic reflector stack have different influence on different modes.

RESULTS AND DISCUSSION

Firstly, the K^2 of these modes with different IDT materials were respectively evaluated. Figure 4 presents the calculated relative admittance as a function of frequency with different IDT materials, Al, Cu and Au, where $h_e = 0.01\ \lambda$, $h_s = 0.2\ \lambda$, $\theta = 42°$. The K^2 of different modes with different IDT materials are listed in the Table 1.

Table indicates that the K^2 of the second mode (SH SAW) is a little larger with better suppression of spurious modes when Au is employed as the IDT material. Consequently, Au was employed as the IDT material for the following calculation. Then, the K^2 and phase velocity (V_p) for the four modes with different electrode and piezoelectric layer thickness in a structure of Au/42° YX-LT/SiO_2/AlN/Diamond have been calculated.

As depicted in Figs. 5a, 5b, where $h_s = 0.2\ \lambda$ and Euler angle $\theta = 42°$, the K^2 for the first and third

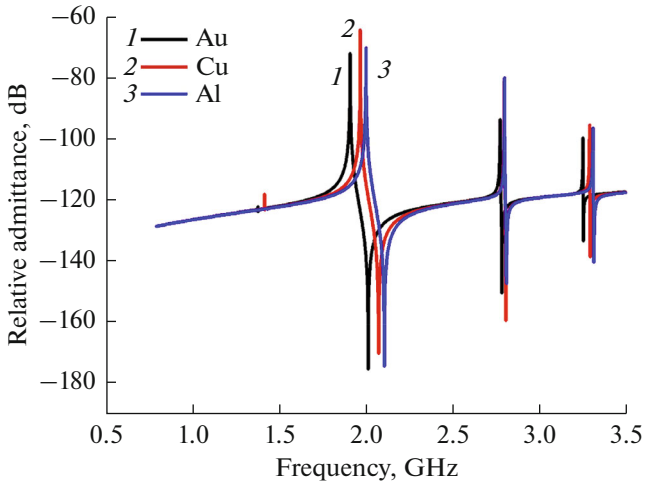

Fig. 4. Relative admittance as a function of frequency for different IDT materials.

modes change little and remain very small values; whereas that for the second and fourth modes change a lot as the h_e increases from 0.01 to 0.1 λ. When h_e ranges from 0.01 to 0.03 λ, the main mode can reach a large value about 12% of K^2 and the spurious modes can be sufficiently suppressed. Furthermore, the K^2 for the main mode can reach its largest value of 12.20% for h_e is 0.02 λ. The phase velocities for all these modes decrease as the h_e increase. Moreover, when the h_e exceeds 0.07 λ, the V_p of the first and second modes, the third and fourth modes, are almost equal to each other, resulting in that they may couple together when propagating in such layered structure.

As depicted in Figs. 6a, 6b, where $h_e = 0.02$ λ and Euler angle θ = 42°, the K^2 for the first mode changes little and remains a very small value, whereas that for the second mode firstly increases, then decreases, and holds a large value. The K^2 for the third mode can achieve a relatively large value at $h_s = 0.3$ λ and $h_s = 0.9$ λ; and the K^2 for the fourth mode can achieve a value of more than 2% for h_s is between 0.3 and 0.8 λ. In summary, for h_s is between 0.1 and 0.3λ, the main mode can reach a large value about 12% of K^2 and the spurious modes can be sufficiently suppressed. Besides, the K^2 for the main mode can reach its largest value of 12.20% for h_s is 0.2 λ. The phase velocities for all these modes decrease as the h_s increases. Moreover, when the h_s gets close to 1 λ, the second and third modes almost couple together.

Table 1. The K^2 of different modes with different IDT materials

	K^2 of the 1st mode	K^2 of the 2nd mode	K^2 of the 3rd mode	K^2 of the 4th mode
Au	0.17%	12.08%	0.88%	0.23%
Cu	0.17%	11.96%	0.87%	0.30%
Al	0.17%	11.79%	0.96%	0.37%

Given the above, when h_e is between 0.01 λ and 0.03 λ, h_s between 0.1 and 0.3 λ, the main mode can achieve a large value of K^2 while the other spurious modes are sufficiently suppressed. Besides, the optimum h_s and h_e are 0.2 and 0.02 λ, where a maximum K^2 of 12.20% and a large phase velocity of 3608 m/s are simultaneously obtained for the main mode.

Finally, the K^2 and effective velocities for the Rayleigh (the first mode) and SH (the second mode) SAWs as a function of Y-cut Euler angle θ from 0° to 180° were calculated while h_s and h_e were 0.2 and 0.02 λ, respectively. The effective velocities are defined by $V_r = f_r\lambda$ and $V_a = f_a\lambda$ at the resonance and anti-resonance frequencies, respectively. As presented in Fig. 7, the pure SH SAW can be obtained with the θ from 0° to 60°, where its K^2 has a wide range of 8.70% to 13.69%. Besides, the K^2 for the SH SAW reaches a maximum value of 13.69% at θ ≈ 25°, then drops to almost zero at θ ≈ 120°, where the K^2 for Rayleigh SAW achieves its maximum value of 1.99%. The effective velocities of the Rayleigh SAW are slower than that of the SH SAW all the time, as a result, they don't couple together.

CONCLUSION

The authors deeply investigated the dependence of K^2 and phase velocities of the different modes propagating in the IHP SAW structure of IDT/θ° YX-LT/SiO_2/AlN/Diamond with different electrode materials and structural parameters. Results show that four eigenmodes simultaneously exist in such layered structure including the main mode SH SAW. Compared with the Traditional SAW structure, it is found that the main mode propagating on the IHP SAW structure could achieve a higher value of K^2 with sacrificing its velocity a little. The relative input admittances for the different IDT materials indicate that the K^2 of the main mode is a little larger with better suppression of spurious modes when Au is employed. Then, the K^2 and V_p for the four modes with different electrode and piezoelectric layer thickness were calculated. Results show that when h_e is between 0.01 λ and 0.03 λ, h_s between 0.1 and 0.3λ, the spurious modes can be sufficiently suppressed. Consequently, the main mode achieves a large value of K^2. Furthermore, the optimum h_s and h_e are 0.2 and 0.02 λ, where a maximum K^2 of 12.20% and a large phase velocity of 3608 m/s for the main mode are simultaneously obtained. The SAWs performance as a function of Y-cut Euler angle θ from 0° to 180° show that the pure SH SAW can be obtained with the θ from 0° to 60°, where its K^2 has a wide range of 8.70% to 13.69%. Such wide

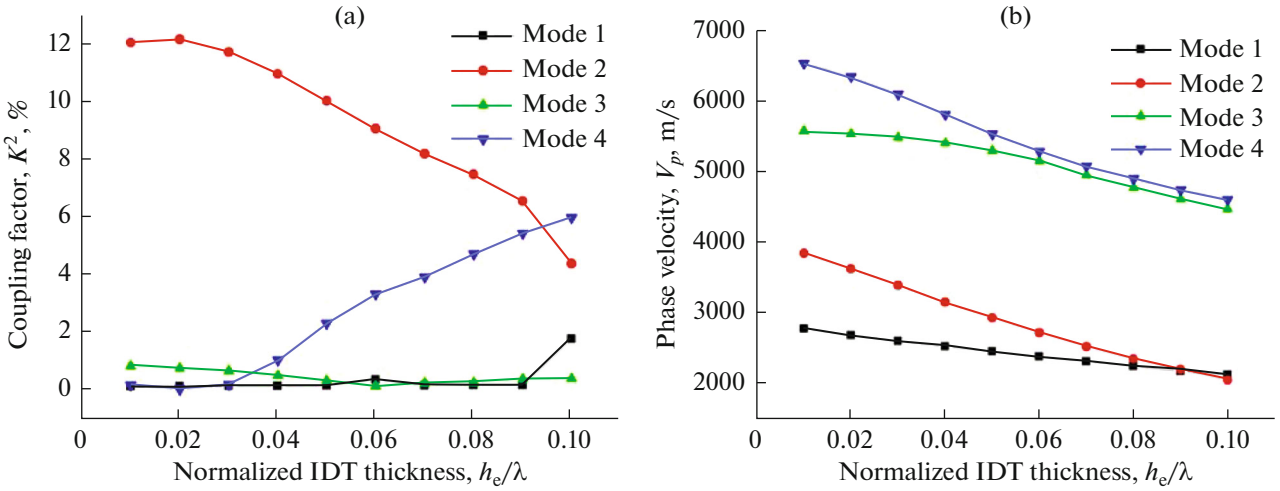

Fig. 5. (a) The K^2 and (b) V_p for the four modes as a function of h_e.

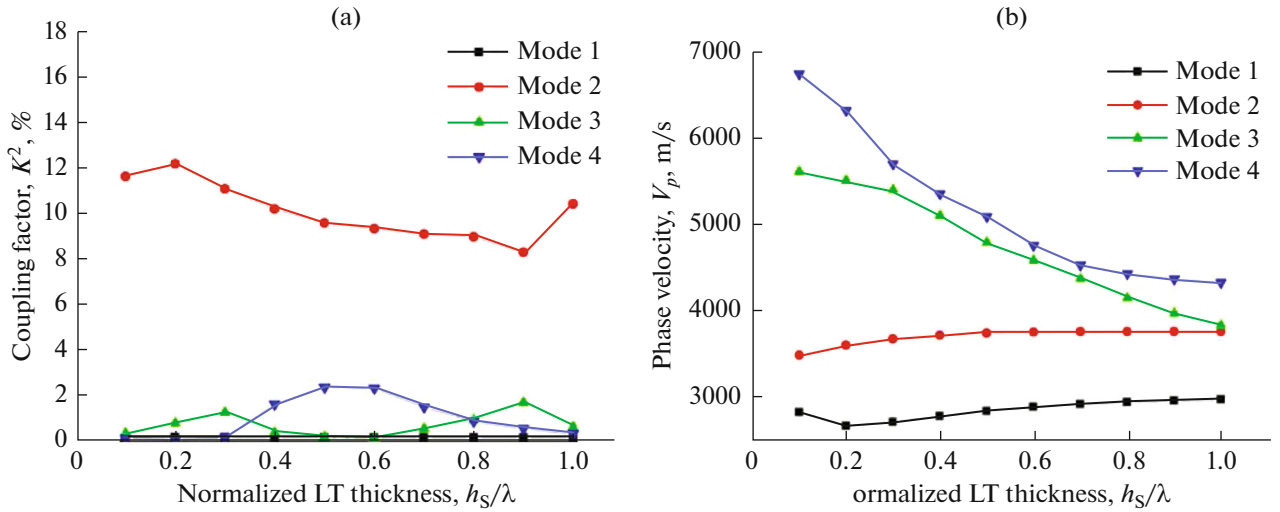

Fig. 6. (a) The K^2 and (b) V_p for the four modes as a function of h_s.

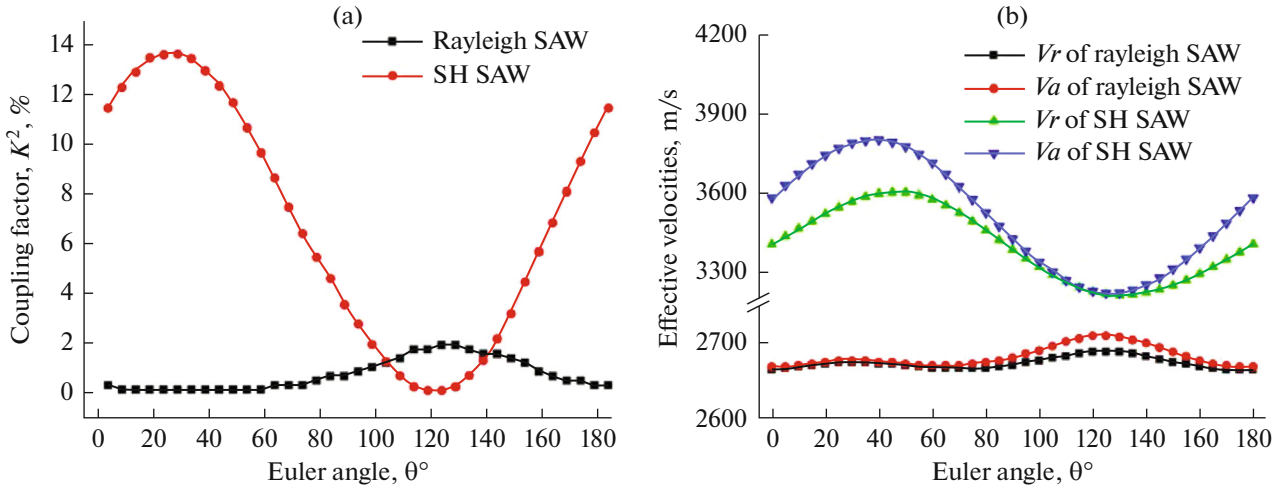

Fig. 7. (a) The K^2 and (b) effective velocities for the Rayleigh and SH SAWs as a function of θ.

range is of great merit for designing different bandwidth of SAW filters. Additionally, the K^2 for the SH SAW reaches a maximum value of 13.69% when $\theta \approx 25°$, then drops to almost zero when $\theta \approx 120°$, at which the Rayleigh SAW achieve its maximum value of 1.99%. Consequently, the work provides a theoretical guide for designing SAW devices of different bandwidth and operation frequency with such structure.

FUNDING

The work was supported by the National Natural Science Foundation of China (NSFC) [grant nos. 51475306, 51705326 and 11404209].

REFERENCES

1. D. I. Makalkin, B. A. Korshak, and A. P. Brysev, Acoust. Phys. **63** (5), 590 (2017).
2. Y. P. Fan and X. J. Ji, Acoust. Phys. **64** (1), 122 (2018).
3. K. Y. Hashimoto, in *Proc. European Frequency and Time Forum* (York, 2016).
4. G. Kovacs, W. Ruile, M. Jakob, U. Rosler, E. Maier, U. Knauer, and H. Zottl, in *Proc. IEEE Ultrasonics Symposium* (Montreal, 2004), Vols. 1–3, p. 974.
5. K. Yamanouchi and S. Hayama, IEEE Trans. Sonics Ultrason. **31** (1), 51 (1985).
6. S. A. Wilkus, C. S. Hartmann, and R. J. Kansy, in *Proc. IEEE Ultrasonics Symposium* (San Francisco, CA, 1985).
7. M. Kadota, T. Nakao, N. Taniguchi, E. Takata, M. Mimura, K. Nishiyama, T. Hada, and T. Komura, in *Proc. IEEE Ultrasonics Symposium* (Honolulu, HI, 2003), Vols. 1–2, p. 2105.
8. M. Kadota, T. Nakao, N. Taniguchi, E. Takata, M. Mimura, K. Nishiyama, T. Hada, and T. Komura, in *Proc. IEEE Ultrasonics Symposium* (Montreal, 2004), Vols. 1–3, p. 1970.
9. M. Miura, T. Matsuda, Y. Satoh, M. Ueda, O. Ikata, Y. Ebata, and H. Takagi, in *Proc. IEEE Ultrasonics Symposium* (Montreal, 2004), Vols. 1–3, p. 1322.
10. X. J. Ji, J. Chen, T. Han, L. Zhou, Q. Z. Zhang, and G. B. Tang, Diamond Relat. Mater. **66**, 213 (2016).
11. M. Akiyama, K. Kano, and A. Teshigahara, Appl. Phys. Lett. **95**, 162107 (2009).
12. B. Abbott and K. Kokkonen, in *Proc. IEEE Int. Ultrasonics Symposium* (Tours, 2016).
13. H. Nakanishi, H. Nakamura, T. Tsurunari, J. Fujiwara, Y. Hamaoka, and K. Hashimoto, Jpn. J. Appl. Phys. **51** (7), 07GC16 (2012).
14. T. Omori, T. Suyama, K. Shimada, C. J. Ahn, M. Yamaguchi, and K. Y. Hashimoto, in *Proc. IEEE Int. Ultrasonics Symposium* (Orlando, FL, 2011), p. 830.
15. T. Takai, H. Iwamoto, Y. Takamine, H. Yamazaki, T. Fuyutsume, H. Kyoya, T. Nakao, H. Kando, M. Hiramoto, T. Toi, M. Koshino, and N. Nakajima, in *Proc. IEEE Int. Ultrasonics Symposium* (Tours, 2016).
16. F. Benedic, M. B. Assouar, P. Kirsch, D. Moneger, O. Brinza, O. Elmazria, P. Alnot, and A. Gicquel, Diamond Relat. Mater. **17** (4–5), 804 (2008).
17. Q. Xiao, C. Dong, X. Ji, P. Cai, and J. Chen, in *Proc. Symposium on Piezoelectricity, Acoustic Waves, and Device Applications* (Chengdu, 2017).
18. S. Fujii and C. Jian, in *Proc. IEEE Int. Ultrasonics Symposium* (Orlando, FL, 2011).
19. M. El Hakiki, O. Elmazria, M. B. Assouar, V. Mortet, L. Le Brizoual, M. Vanecek, and P. Alnot, Diamond Relat. Mater. **14** (3–7), 1175 (2005).
20. X. G. Tian, L. Q. Tao, B. Liu, C. J. Zhou, Y. Yang, and T. L. Ren, IEEE Electron Device Lett. **37** (8), 1063 (2016).
21. J. Bjurstrom, G. Wingqvist, V. Yantchev, and I. Katardjiev, J. Micromech. Microeng. **17** (3), 651 (2007).
22. K. Hashimoto, H. Asano, T. Omori, and M. Yamaguchi, Jpn. J. Appl. Phys. **43** (5b), 3063 (2004).
23. D. A. Gubaidullin and Y. V. Fedorov, Acoust. Phys. **64** (2), 164 (2018).
24. M. L. Amamou, Acoust. Phys. **62** (3), 280 (2016).